ELSEVIER

Catalysis Today 44 (1998) 357–368

CATALYSIS TODAY

A new photocatalytic reactor for destruction of toxic water pollutants by advanced oxidation process

Ajay K. Ray*

Department of Chemical Engineering, National University of Singapore, 10 Kent Ridge Crescent, Singapore 119260, Singapore

Abstract

A new photocatalytic reactor design for water treatment is presented, characterized by the use of new extremely narrow diameter lamps, thus allowing for much higher surface area for catalyst coating per unit reactor volume and consequently for much higher specific reactor capacity. Experiments in a reactor containing 21 novel U-shaped lamps coated with the catalyst showed 695% increase in efficiency of the reactor performance when compared with classical annular reactor, 260% when compared with a slurry reactor, and 60% when compared with a multiple tube reactor. The classical annular reactor and slurry reactor cannot be scaled-up for large-scale applications due to the low values of an illuminated catalyst surface area per unit volume of liquid treated inside the reactor. In the multiple tube reactor the above problem could be eliminated, but it suffers from the disadvantage that uniform light intensity cannot be achieved. Development of a reactor using the new lamps will provide all the advantages of the multiple tube reactor, plus the additional advantage that the catalyst could be activated at its highest level. The present configuration is flexible enough for large-scale applications.

Keywords: Semiconductor photocatalysis; Titanium dioxide; Water treatment

1. Introduction

The presence of harmful impurities in water supplies and in the discharge of wastewater from chemical industries, power plants and agricultural sources is a topic of global concern [1,2]. All existing water treatment processes, currently in use, have limitations of their own and none is cost-effective. In recent years, heterogeneous photocatalysis [3,4] that couples low energy ultraviolet light with semiconductors acting as photocatalysts has emerged as a viable alternative for the traditional water treatment methods. The appeal of this process technology is the prospect of complete mineralization of the pollutants into a harmless compound [5].

Activation of the catalyst is achieved by electron–hole pair formation initiated through the absorption of a photon of ultraviolet band-gap energy [6]. Of all the different semiconductor photocatalysts tested, TiO_2 appears to be the most active [5]. TiO_2 photocatalysis is more appealing because it is cheap, biologically and chemically inert, photostable, nontoxic, can be used for extended period without substantial loss of its activity, and requires only about 1 W/m^2 light [7]. The catalyst can even be activated with sunlight [8].

*Corresponding author. Tel.: 00 65 874 8049; fax: 00 65 779 1936; e-mail: cheakr@nus.edu.sg

0920-5861/98/$32.00
PII S0920-5861(98)00210-7

Inspite of the potential of this promising technology, development of a practical water treatment system has not yet been successfully achieved. In the last few years, a large number of publications have appeared based on laboratory scale studies with generally positive results for very diverse categories of toxic compounds in water. However, technical development to pilot scale level has not yet been successfully achieved although there are numerous patents approved all over the world [9].

There are several factors that impede the efficient design of photocatalytic reactors. In this type of reactors, besides conventional reactor complications such as mixing, mass transfer, reaction kinetics, catalyst installation, etc., an additional engineering factor related to illumination of catalyst becomes relevant. The high degree of interaction between the transport processes, reaction kinetics and light absorption leads to a strong coupling of physico-chemical phenomena. The illumination factor is of utmost importance since the amount of catalyst that can be activated determines the water treatment capacity of the reactor [9].

The central problem of scale-up of photocatalytic reactor is focused on providing high specific catalyst surface area and uniform distribution of light for catalyst illumination. The first problem could be avoided by packing the reactor with large numbers of catalyst coated hollow tubes [9], while the second problem could be eliminated by using extremely narrow diameter novel lamps coated on its surface with catalyst as presented in this paper. The present paper describes a new reactor design based on extremely narrow diameter novel lamps that allows for a much higher illuminated surface area per unit reactor volume and is flexible enough to be scaled-up for commercial scale applications.

2. Basic concept of the reactor

The concept is based on a unique new lamp design developed by Philips. These are extremely narrow diameter fluorescent tube lamps of low wattage emitting lights in the wavelength of our interest (λ<380 nm). These lamps are available in various shapes and lengths, and can be placed inside a reactor to form a variety of different configurations. The photocatalytic reactor is described here as tube light reactor (TLR). Since the lamps are extremely narrow in diameter, evidently a very large number of such lamps can be placed inside the reactor. In the present reactor configuration, the catalyst was deposited on the outer surface of these low wattage lamps and thus provides a high light transfer area and allows for a higher illuminated specific catalyst surface area than even a slurry reactor. Another potential advantage of distributing light is that light does not have to pass through the reactant and product phases in the reactor. This is advantageous because when light approaches the catalyst through the bulk liquid phase, some radiation is lost due to absorption in the liquid. This effect is more pronounced for highly colored dye pollutants as they are strong UV absorbers and will therefore, significantly screen the TiO_2 from receiving UV light. Of course, this is possible with classical lamps too. However, the new lamps allow for a 10–20 times larger surface area for catalyst per unit reactor volume compared to a classical reactor design (Table 1).

3. Experimental

3.1. The reactor

The reactor, see Fig. 1, consists of a stainless steel flat top plate (0.132 m×0.016 m) with 21 holes onto which another plate (0.248 m×0.132 m) was welded. Twenty-one U-shaped lamps were placed around the latter plate and its end extended through the holes for electrical connections. Electrical wires were connected to the novel lamps through copper holders that are screwed around the lamp's end. This part acts as a clamp for the lamps. The assembly was put in a rectangular stainless steel reactor vessel. Feed is introduced at the top of the vessel and is equally distributed over the width of the reactor through five inlet ports thereby minimizing the formation of any dead zones. Similarly, the flow exits the reactor through five ports at the other end. The effective illuminated surface areas of the catalyst and the volume of the reactor are 0.15 m^2 and 5.36×10^{-4} m^3, respectively. The parameter κ, defined as total illuminated catalyst surface area that is in contact with reaction liquid per unit volume of liquid treated in the reactor volume, is equal to 618 m^2/m^3.

Table 1
Comparison of illuminated catalyst surface area per unit volume of liquid treated inside the reactor, κ (m^2/m^3) for different reactors

Photocatalytic reactor	κ (m^2/m^3)	Parameters	κ (m^{-1})	Remarks
Slurry reactor	$\left[\frac{6C_c}{\rho_c}\right]\frac{1}{d_p}$	d_p=0.3 μm, C_c=0.5 kg/m^3	2631[a]	Scale-up not possible
External type – annular reactor	$\frac{4d_0}{d_0^2 - d_i^2}$	d_0=0.2 m, d_i=0.1 m	27	Scale-up not possible
Immersion type – with classical lamps	$\left[\frac{4\epsilon}{1-\epsilon}\right]\frac{1}{d_0}$	d_0=0.09 m, ϵ=0.75	133	Scale-up possible but large V_R
Distributive type – with hollow tubes	$\left[\frac{4\epsilon}{1-\epsilon}\right]\frac{1}{d_0}$	d_0=0.006, ϵ=0.75	2000	Scale-up possible with small V_R
Immersion type – with new lamps	$\left[\frac{4\epsilon}{1-\epsilon}\right]\frac{1}{d_0}$	d_0=0.0045, ϵ=0.75	2667	Scale-up possible with small V_R

[a]The value will be much lower than 2631 m^{-1} as all the suspended catalyst particles will not be effectively illuminated. Catalyst concentration, C_c, of 0.5 kg/m^3 is normally used. ρ_c is equal to 3800 kg/m^3.

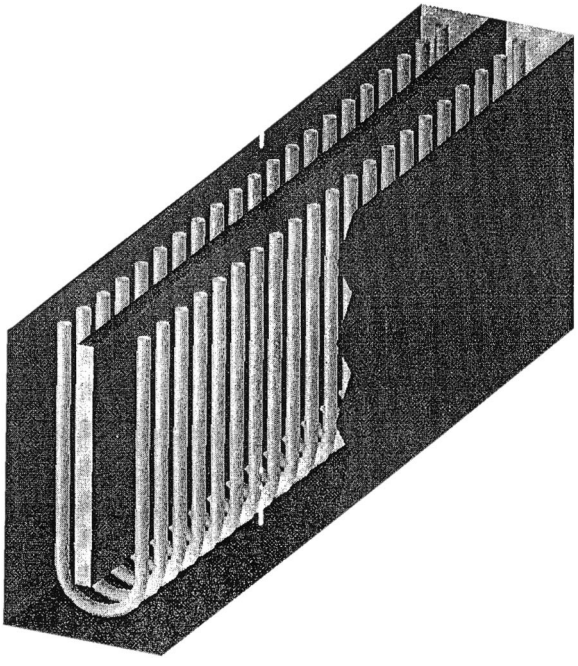

Fig. 1. Schematic diagram of tube light reactor (TLR).

3.2. Lamps

The novel lamps (Philips NDF-U2 49-6W) used were specially developed by Philips Lighting for our experiments. The U-shaped lamps are 0.498 m long and have a diameter of 0.0045 m only. These operate at 1020 V; produce 6 W of which 15% is in the UV-A region. The light intensity (λ<380 nm) on catalyst particles is 127.8 W/m^2.

3.3. Experimental set-up

A gear pump (Verder model 2036; maximum flow rate of 3.0×10^{-5} m^3/s) circulated the reactant between the reactor and the reservoir via a flow-through cuvette placed inside a photometer (Vitatron 6000) for continuous on-line measurement of the model component (Fig. 2). Two three-way glass valves were used between the water and specially designed reactant reservoir for initial zero-setting of the analytical instrument before the start of an experiment, introduction of the reactant into the system, elimination of bubbles formed during experiment, and final flushing of the entire system. The reactor assembly was placed inside a thermostat bath.

3.4. Catalyst

Degussa P25 grade TiO_2 was used as the catalyst for all the experiments. The crystalline product is non-porous primarily in the anatase form (70:30 anatase to rutile) and is used without further treatment. It has a BET surface area of $(5.5\pm1.5)\times10^4$ m^2/kg and crystallite sizes of 30 nm in 0.1–0.3 μm diameter aggregates.

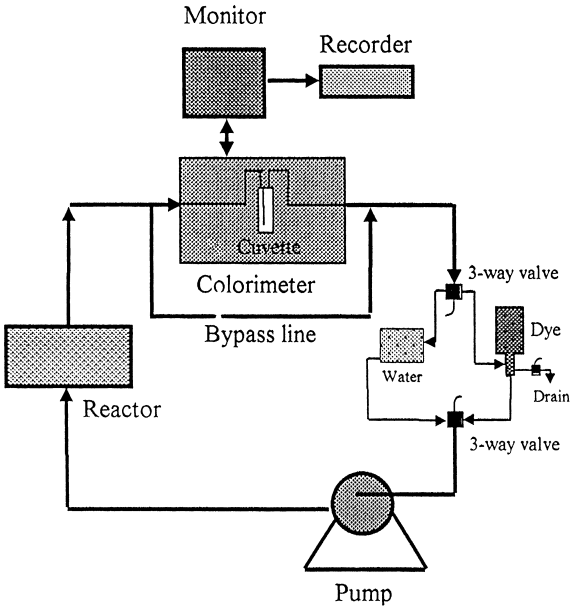

Fig. 2. Flow diagram of the experimental set-up.

3.5. Catalyst immobilization

For better catalyst fixation and its durability, the glass surface of the lamps was roughened by sand blasting. This makes the catalyst surface uneven but increases the strength and amount of catalyst per unit area that could be deposited. The lamp surface was carefully degreased, cleaned with 5% HNO_3 solution overnight, washed with water and then dried. A 5% aqueous suspension of the catalyst was prepared with water out of Millipore Milli-Q water purification system. The suspension was mixed in an ultrasonic cleaner (Branson 2200) bath to obtain a milky suspension that remained stable for weeks. The lamp's surfaces were coated with catalyst by a dip-coating apparatus (Fig. 3) designed for coating the catalyst. This is a completely automated equipment capable of immobilizing catalyst onto a variety of different shaped and sized substrates to any desired thickness by successive dipping of the objects into a suspension at controlled speed that can be varied between $(0.4–4.0)\times10^{-4}$ m/s. Four 250 W infrared lamps were attached to a clamp that can be moved both vertically and horizontally for instant drying of the coating. Fig. 4 shows the amount of catalyst immobilized per unit area with the number of dippings.

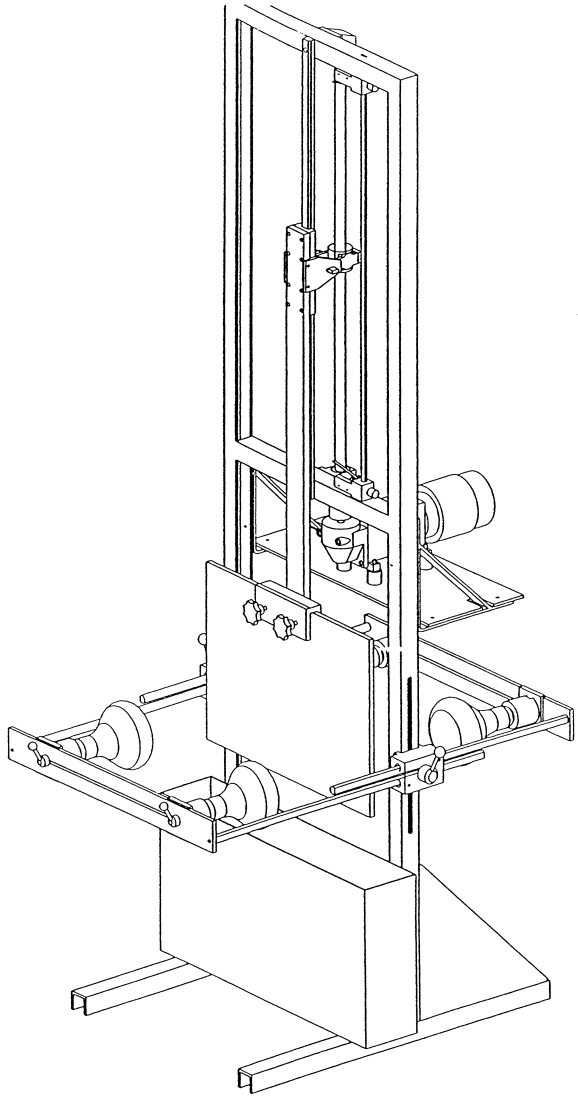

Fig. 3. Dip-coating apparatus.

3.6. Model component

Special Brilliant Blue of Bayer (SBB, MW 812), of laboratory reagent grade (in 20% solution) was used (catalog number 42735). This is an excellent model component for characterization of a photocatalytic reactor [10] as the dye is reactive only in presence of both TiO_2 and UV light, biologically not degradable, and present in wastewater streams from textile industries. The complete oxidation reaction of

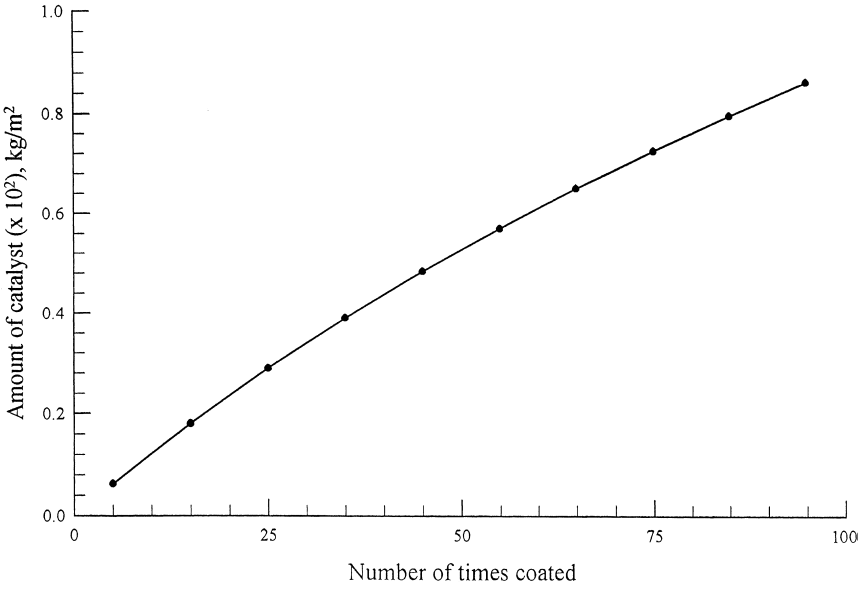

Fig. 4. Catalyst layer thickness with number of coatings.

SBB dye is

$$C_{43}H_{71}O_6N_3S_2Na + 64\tfrac{1}{2}O_2 \rightarrow 43CO_2 + 32H_2O + 2H_2SO_4 + 3HNO_3 \quad (1)$$

3.7. Analysis

Changes in SBB dye concentration were measured on-line by flowing a bypass stream of the dye from reactor outlet continuously through a bottom loader flow-through cuvette (Hellma, path length 0.001 m) placed inside a colorimeter (Vitatron Universal Photometer 6000) and was recorded continuously by a Kipp&Zonen (Model BD80) recorder. Up to 0.5 mol/m^3, the calibration line obeys the Beer–Lambert law with good precision and the absorptivity coefficient, ϵ (at λ_{max}=605 nm), was found to be 5000 m^3/mol/m.

3.8. Experimental procedure

At the start of every experiment the reactor was rinsed with Milli-Q water before zero-setting the analytical instrument. The reactor was then filled with the dye solution and it was ensured that no air bubbles remained in the system. The change in the dye concentration was continuously recorded. New silicon connecting tubes and fresh catalyst were found to adsorb the dye for about an hour, but no noticeable adsorption by the entire system was observed afterwards. Light was turned on only when the colorimeter reading was stabilized. A typical experimental result is shown in Fig. 5. The decrease in concentration in the first two parts can be attributed to the adsorption of the dye by the connecting tubing (no catalyst present) and fresh catalyst, respectively, while that of the last part was when light was turned on and actual photocatalysis occurred.

3.9. Evidence of complete mineralization

The COD for SBB dye is given by

$$\mathrm{COD} = y \cdot [M_{\mathrm{Oxygen}}/M_{\mathrm{SBB\ dye}}]. \quad n = 2.542\ y \quad (2)$$

where y is the concentration of the SBB dye in ppm, M_{Oxygen} and M_{SBB} dye are the respective molecular weights and n for the dye is $64\frac{1}{2}$. COD was measured for various virgin dye solutions, for liquid collected at the end of several experiments and for pure Milli-Q water. COD values for the virgin solutions were always equal to the value calculated from Eq. (2) and that of the treated liquid and blank were zero. COD value for the final treated liquid shows that

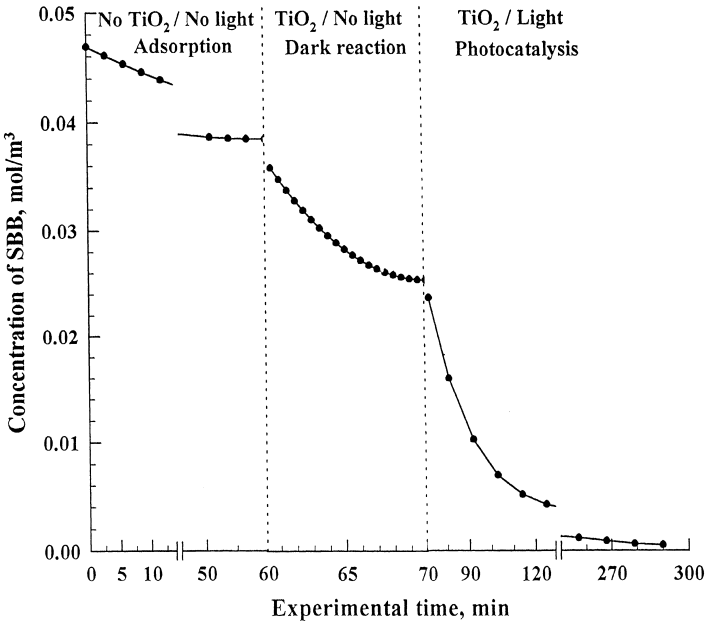

Fig. 5. Typical experiment showing adsorption of the dye in the system, dark reaction and photocatalysis.

complete mineralization occurred and for the present model component colorimetric analysis was justified as it was not merely measuring the decolorization of the dye.

3.10. Reaction mechanism

It has been well demonstrated that when TiO_2 is illuminated by light (λ<380 nm) in the presence of water containing dissolved oxygen and organic compounds, photodegradation of the organic compounds will occur. Many organic compounds are known to be degraded to CO_2 under these conditions. The primary step in photodegradation is certainly the generation of electrons and holes within the TiO_2 particle:

$$TiO_2 \overset{h\nu,\ \lambda<380\,nm}{\rightarrow} TiO_2\ (e^- + h^+) \quad (3)$$

The majority of these recombine with the liberation of heat. However, in the presence of dissolved oxygen and an electron donor, $OH^{\bullet}$ radical is formed by the reaction between the valence band holes (h^+) and the TiO_2 surface active $OH^{\bullet}$ group or H_2O:

$$h^+ + OH^{\bullet} \rightarrow OH^{\bullet}_{ad} \quad (4)$$

$$h^+ + H_2O_{ad} \rightarrow HO^{\bullet}_{ad} + H^+ \quad (5)$$

The photogenerated conduction band electron (e^-) is trapped by the dissolved oxygen to form a superoxide ion O_2^-:

$$e^- + O_2 \rightarrow O_2^{\bullet -} \quad (6)$$

The dye will be attacked by hydroxyl radicals formed in the above equations and generates organic radicals or some other intermediates. NO_2^- was found and oxidized to NO_3^- while SO_3^- was found and oxidized to SO_4^- [10]. Eventually all the parent compounds and intermediates will be oxidized into CO_2 with an overall reaction stoichiometry described by Eq. (1)[7].

The pH value is an important parameter in photodegradation that takes place on the surface of the photocatalyst. The point of zero charge (pzc) for TiO_2 is at pH between 5.6 and 6.4 [11]. Hence, at more acidic pH values, the catalyst surface is positively charged, while at pH values above 5.6, it is negatively charged. Therefore, pH value has a significant effect on the adsorption–desorption properties at the catalyst's surface.

The effect of pH on the degradation of the dye shows that pH value has a significant effect and at both low and high pH values photodegradation rates are quite slow [7]. The best pH value for the degradation is

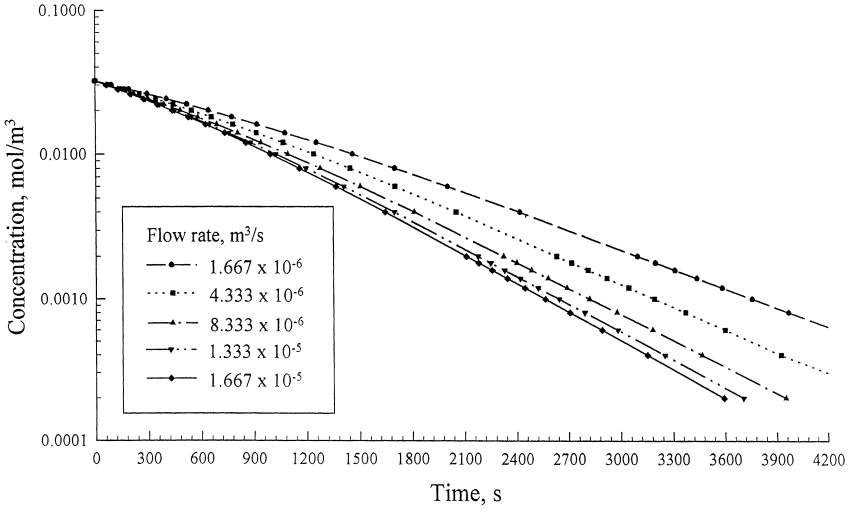

Fig. 6. Influence of external mass transfer (flow rate) on the overall rate.

near the pzc point of TiO_2. This probably explains that the effect of pH on degradation rate is perhaps due to its effect on TiO_2 particle itself [10].

3.11. Experimental results

Experiments with increased flow rate caused an increase in the conversion rate (Fig. 6) showing influence of external mass transfer. For most experiments a flow rate of 1.67×10^{-5} m^3/s was used as higher flow rates introduced bubbles inside the reactor.

Fig. 7 shows experimental results for the photocatalytic destruction of SBB for various starting concentrations. The figure reveals that 90% of the pollutant was degraded in about 30 min. The efficiency of the reactor, expressed in terms of mols converted per unit time per unit reactor volume per unit electrical power consumed, is compared with three different reactors, namely a slurry reactor [12], a classical annular reactor [12], and a multiple tube reactor [9] for the same initial concentration (C_0=0.024 mol/m^3) of the SBB dye. The slurry reac-

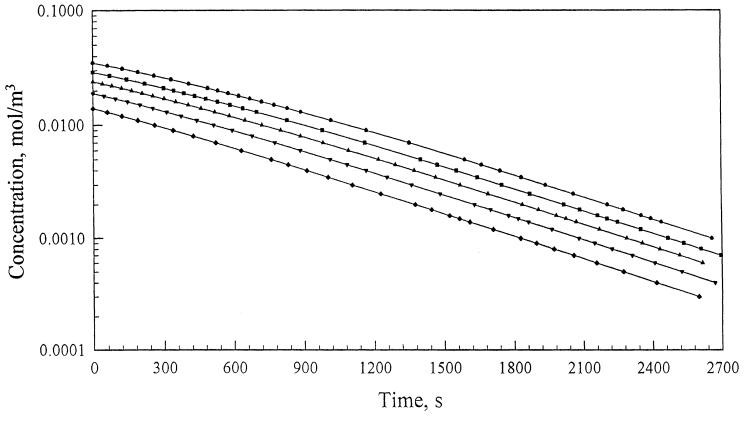

Fig. 7. Photocatalytic degradation of SBB dye for various initial concentration. (Reactor specification: volume of reactor=5.36×10^{-4} m^3; illuminated catalyst surface area=0.15 m^2; number of lamps=21; catalyst amount=4.0×10^{-3} kg/m^2; experimental condition: flow rate=1.67×10^{-5} m^3/s; volume of liquid treated=4.05×10^{-4} m^3.)

Table 2
Comparison of reactor specifications, experimental conditions and reactor performance efficiency for classical annular reactor (CAR), slurry reactor (SR) and tube light reactor (TLR)

	Classical annular reactor (CAR) [12]	Slurry reactor (SR) [12]	Multiple tube reactor (MTR) [9]	Tube light reactor (TLR)
Volume of reactor, m^3	3.48×10^{-3}	1.4×10^{-3}	1.23×10^{-3}	5.36×10^{-4}
Catalyst surface area, m^2	0.18	3.7	0.51	0.15
Parameter κ, m^2/m^3	69	6139[b]	1087	618
Volumetric flow rate, m^3/s	8.42×10^{-5}	Batch operation	3.00×10^{-5}	1.67×10^{-5}
Electrical energy input, W	400	960	40	126
Efficiency[a], $\mu mol/s/m^3/W$	9.50×10^{-3}	2.10×10^{-2}	5.09×10^{-2}	7.55×10^{-2}
Increase in efficiency, %	1	121	436	695
Scale-up possibilities	No	No	Yes	Yes

[a]Efficiency is expressed as 90% pollutant (SBB dye) converted (μmol/s) from a starting concentration of 0.024 mol/m^3 per unit reactor volume (m^3) per unit electrical energy (W) used.
[b]The value will be much lower than 6139 m^{-1} as all the suspended catalyst particles are not effectively illuminated and the assumption of the average aggregate particle diameter of 0.3 μm may be too small.

tor consists of 20 tubes each of volume 7×10^{-5} m^3 containing 3×10^{-5} m^3 of liquid (with TiO_2 concentration of 0.5 kg/m^3) placed on a holder that rotates around a magnetic stirrer and was surrounded by 24 Philips TLK 40W/10R lamps. The annular reactor was of 0.099 m outside and 0.065 m inside diameter with 0.77 m long surrounded externally with 10 Philips TLK 40W/10R lamps. While the multiple tube reactor [9] consisted of 54 hollow tubes of 0.006 m diameter coated with the catalyst on its outer surface and was densely packed in a reactor of 0.06 m diameter and 0.5 m long. When the efficiency of the test reactor is compared (Table 2) with the classical annular reactor an increase of about 695% was observed while an increase of 259% was observed when compared to the slurry reactor inspite of the fact that slurry reactor offers much higher κ value. The efficiency improvement for the present reactor over MTR [9] is about 60% greater because of the superior catalyst activation. This increase in efficiency is inspite of the fact that the design of this test reactor was far from optimum with respect to mass transfer, flow distribution and efficiency of packing of the tube lamps inside the reactor. In addition, the novel reactor design has the capability of scaled-up to any dimensions whereas the first two reactors are restricted only to a small reactor capacity.

The catalyst coating on the lamp's surface appeared to be durable and the catalyst activity did not deteriorate even after 50 h of experimentation. One problem is still the burning stability and lifetime of the lamps but it is expected that this will be improved in the months ahead. A comprehensive experimental program on the influence of operating parameters on the conversion rates is presently being carried out. It is apparent that MTR design idea creates great opportunities for building much more efficient photocatalytic reactor for water purification, as the reactor will definitely be economical compared to other photocatalytic reactor.

The main obstacle in the development of MTR design concept [9] was that it was impossible to obtain uniform light distribution along the length of the tubes and thereby severely restricting the maximum length of tubes that could be used. One way of avoiding this will be to place one such extremely narrow diameter novel lamp inside each of the hollow tubes. In this way all the advantages of the MTR concept can be utilized while eliminating the basic drawback of uniform light distribution dilemma. Moreover, this will also eliminate the main problem experienced with the prolonged use of the novel lamps in the present reactor. It was observed in the TLR that the performance of the lamps deteriorates with time due to its operation immersed in polluted water.

4. Numerical simulation of the reactor

Although experimental results are very promising, it is observed that the overall destruction rate is limited to mass transport of the pollutant to the catalyst sur-

face. The reaction occurs at the liquid–solid interface and mass transfer from the bulk of the liquid to the catalyst surface plays an important role in the overall rate. Numerical simulation of the reactor is being performed using a commercial CFD package FLUENT to determine effects of flow rates, diffusion coefficients, reaction rate constants, and inter-lamp spacing on the conversion of pollutants.

The present reacting flow model solves the transport equations (pressure and u-, v-, w- momentum) and species conservation equations. When the turbulence model is activated, an additional two equations (for k and ϵ) need to be solved. For an accurate solution these highly nonlinear and coupled equations are solved at each cell (or grids) for each iteration. This type of computation demands very high memory and CPU speed, which normally exist in expensive parallel supercomputers.

In order to get accurate results, the 3D model of the reactor requires control volume ranging from 500 000 to 1 000 000 cells and the computation had to be carried out for at least 2000 iterations to obtain converged solution. This is not only very time consuming as it requires about 10 days on a single SGI workstation, but also it may not always be possible to read the entire problem into the computer's random access memory (RAM). A state-of-the-art efficient computational method, namely, parallel processing on a distributed computing environment, was employed to expedite the calculation and overcoming the memory bottleneck present in a single workstation.

4.1. *Parallel processing on a distributed computing environment*

Unlike normal computers, which do calculations sequentially, parallel computers break up a task into parts and then perform them simultaneously that has a single cabinet with multiple CPUs connected to a large set of memory. Distributed computing differs from parallel computing in the sense that a set of computers connected by a network are used collectively to solve a single large problem by distributing the load among all the processors. In order to solve the problem using distributive computing, the grid was partitioned into multiple subdomains such that the number of partitions is an integral multiple of the number of compute nodes available. In general, as the number of compute node increases, turnaround time for the solution will decrease. However, parallel efficiency decreases as the ratio of communication to computation increases. In this paper, four SGI workstations (compute nodes) with different types of configurations were interconnected to act as a single virtual machine. Typical partitioning of the grid is shown in Fig. 8, where the entire domain is partitioned into four subdomains.

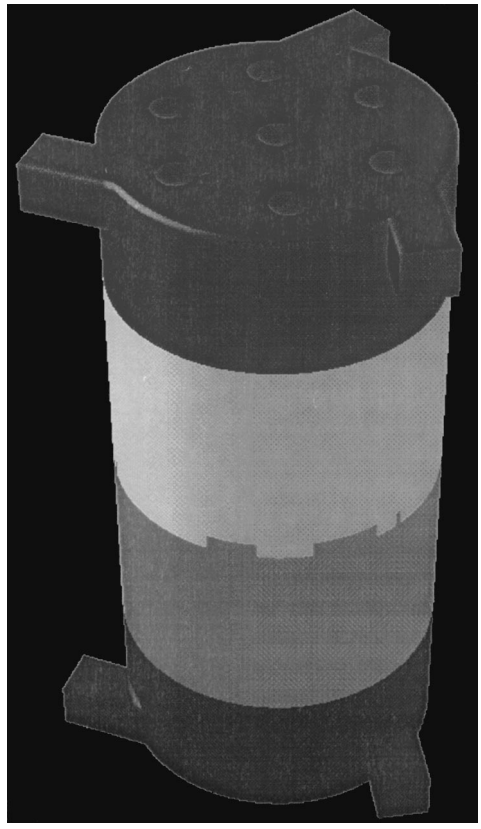

Fig. 8. Photocatalytic reactor geometry and domain decomposition for the purpose of parallel processing on a distributed computing environment. The mesh is partitioned into four sub-domains.

Partitioning was done with serial version of Fluent/UNS, and then it was read into the parallel solver. Partitioning of the grid was executed automatically once the number of subdomains was specified. The partitioning processing has three major goals:

1. creating partitions with equal numbers of cells,
2. minimizing the number of partition interfaces, i.e., decrease partition boundary surface area, and
3. minimizing the number of partition neighbors.

Balancing the partitions (equalizing the number of cells) ensures that each processor has an equal load and that the partitions will be ready to communicate at about the same time. Since communication between partitions is a relatively time-consuming process, minimizing the number of interfaces reduces the time associated with this data interchange. Minimizing the number of partition neighbors reduces the chances for network and routing contentions. In addition, minimizing partition neighbors is important on machines where the cost of initiating message passing is expensive compared to the cost of sending longer messages.

4.2. Discussions of simulation results

Initially a reasonably converged solution was obtained for the velocity and pressure equations. The reaction part of the solver was then activated, and using the almost converged solution as the initial condition, a complete solution of the reacting flow model was obtained. The converged velocity profiles at various regions of the reactor were observed to determine the degree of mixing. Fluid mixing is one of the important criteria in efficient photocatalytic reactor design as the transport of reactants from the bulk of the liquid to the catalyst surface determines the extent of fluid–catalyst contacting and overall conversion. Streaklines were used to determine the degree of mixing inside the reactor (Fig. 9). The streakline pattern shows that maximum mixing takes place at the bottom of the reactor where fluid enters the reactor tangentially with a swirling motion. There is also a good degree of mixing just before the fluid exits at the top of the reactor. However, the flow is quite uniform without much mixing in the mid-region between the inlets and outlets.

The advantage of using computer simulations is that the length of the reactor required for complete degradation of a particular pollutant can be determined easily compared to time-consuming expensive experimental studies. In addition, the flexibility of determining the effects of various process parameters in computer simulations will be useful, particularly flow rates, as the degradation rate strongly depends on the residence time of the fluid inside the reactor. A typical case of degradation of the dye pollutant and formation of carbon dioxide is shown in Fig. 10(a) and (b). The figure shows that most of the dye can be degraded when the flow rate used was 6 cm^3/s, thereby indicating that the reactor could be used for treating larger capacity if simultaneous increase in mixing and residence time of the pollutant inside the reactor is improved.

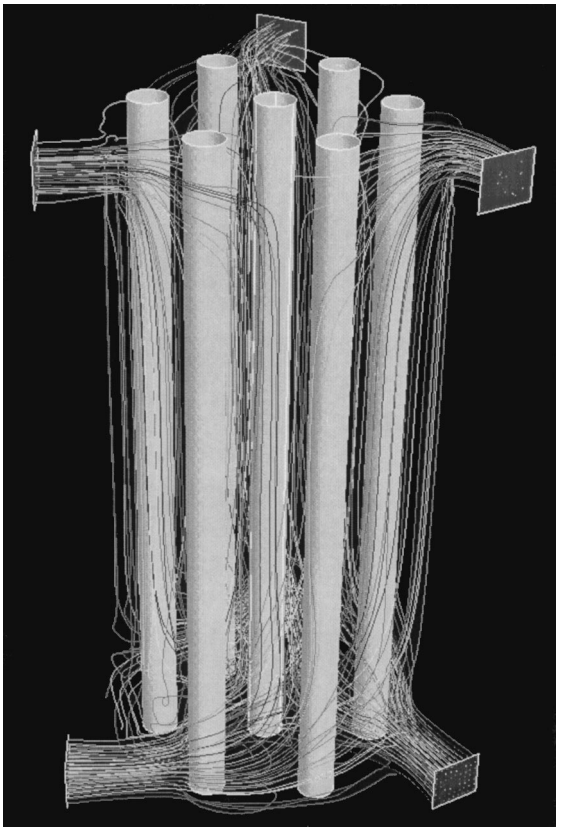

Fig. 9. Streaklines show the degree of mixing inside the reactor.

5. Conclusions

A new photocatalytic reactor design concept with a 100–150-fold increase in surface area per unit volume of reaction liquid inside the reactor relative to a classical annular reactor design and a 10–20-fold increase relative to an immersion type reactor with classical lamps has been proposed and developed. Experimental results based on a reactor configuration where new extremely narrow diameter artificial fluor-

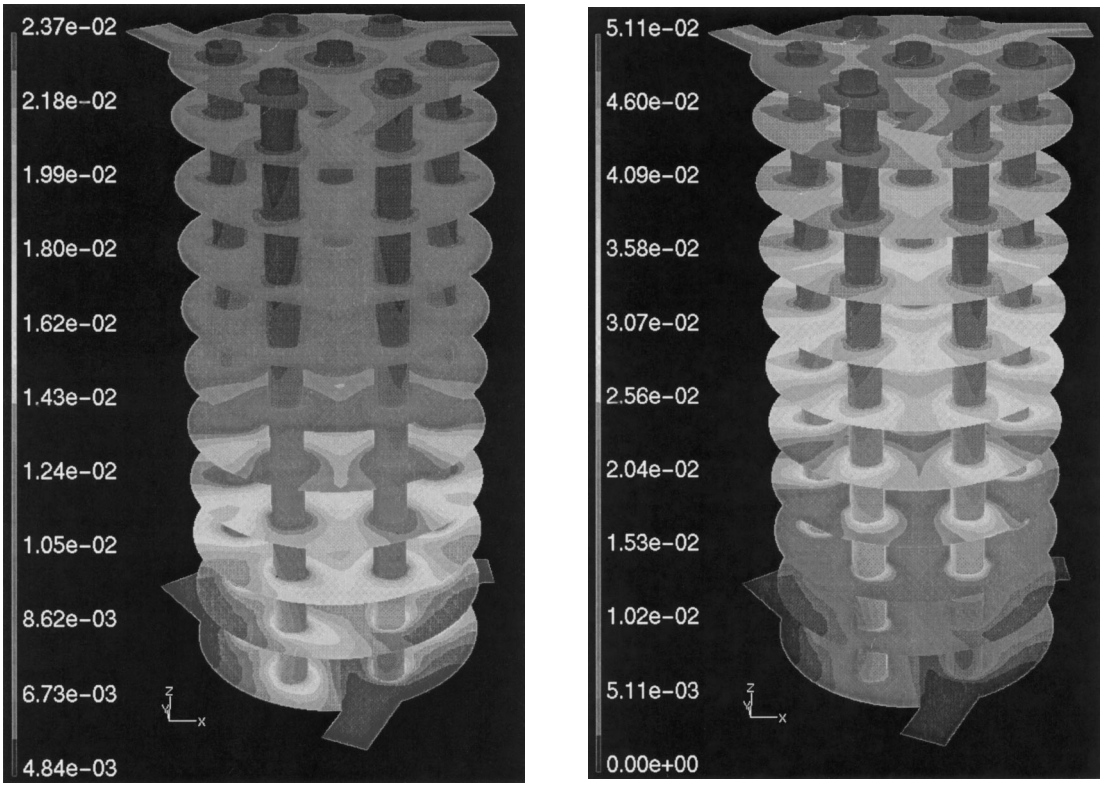

Fig. 10. (a) Contour concentration plots of SBB dye degradation in the photocatalytic reactor. The flow direction is from bottom to top. (b) Contour concentration plots of CO_2 formation in the photocatalytic reactor. The flow direction is from bottom to top.

escent lamps with near UV spectra are used is presented. A simple laboratory-scale test reactor using these lamps was designed, constructed and tested for an overall performance evaluation. Experiments performed in a reactor of volume 5.36×10^{-4} m^3 containing 21 novel U-shaped lamps of diameter 0.0045 m coated with the catalyst showed 695% increase in efficiency of the reactor performance when compared with classical annular type photocatalytic reactor, 259% when compared with a slurry reactor, and 60% increase when compared with multiple tube reactor. Both classical annular reactor and slurry reactor cannot be scaled-up for large-scale applications due to the low values of illuminated catalyst surface area per unit volume of liquid treated inside the reactor while the present configuration is flexible enough for industrial scale applications. The computer simulation is currently being used to fine tune the reactor design to achieve better fluid–catalyst contacting to minimize mass transfer limitation, and simultaneous increase of flow rate to increase the capacity of water treatment by the reactor and increase of residence time to increase the conversion rate of the pollutant.

References

[1] O. Legrini, E. Oliveros, A.M. Braun, Chem. Rev. 93 (1993) 671.
[2] M.R. Hoffmann, S.C. Martin, W. Choi, D.W. Bahnemann, Chem. Rev. 95 (1995) 69.
[3] D.F. Ollis, E. Pelizzetti, N. Serpone, Photocatalysis: Fundamentals and Applications, Wiley, New York, 1989.
[4] A. Hagfeldt, M. Grätzel, Light-induced redox reactions in nano-crystalline systems, Chem. Rev. 95 (1995) 49.
[5] A. Mills, R.H. Davies, D. Worsley, Chem. Soc. Rev. (1993) 417.
[6] M.A. Fox, M.T. Dulay, Chem. Rev. 93 (1993) 341.

[7] A.K. Ray, A.A.C.M. Beenackers, AIChE J. 43(10) (1997) 2571.
[8] W.A. Zeltner, C.G. Hill, M.A. Anderson, CHEMTECH (1993) 21.
[9] A.K. Ray, A.A.C.M. Beenackers, Catal. Today 40 (1998) 73.
[10] D. Chen, A.K. Ray, Water Res., in press, 1998.
[11] R. Terzian, N. Serpone, J. Photochem. Photobiol. A 89 (1995) 163.
[12] J.W. Assink, T.P.M. Koster, J.M. Slaager, Internal report ref. no. 93-137 1993, TNO Milieu en Energie, Apeldoorn, Netherlands, 1993.